Journal of Engg. Research **Vol. 6 No. (3) September 2018 pp.** *203-224*

Numerical simulation of static and dynamic aerodynamics for formation flight with UCAVs

Baigang Mi*, Hao Zhan and Baibing Chen**

* *School of Aeronautics, Northwestern Polytechnical University, Xi'an, China*

** *Xi'an Modern Control Technology Research Institute, Xi'an, China*

* *Corresponding Author: mibaigang@sina.com*

ABSTRACT

Using the effect of wingtip vortex from a leading aircraft, the formation flight of unmanned combat aerial vehicles (UCAVs) can accomplish various tasks with much more efficiency. Combined with the sliding mesh technique, this paper investigates a computational fluid dynamics (CFD) method to simulate and analyze, in detail, the static and dynamic aerodynamic characteristics of formation with two flying wing models named as SACCON. Besides, the dynamic derivatives indicating the dynamic stability of aircrafts in formation are identified and validated, and normal single flights are also analyzed as a comparative study. The results demonstrate that, due to the wake of the leader, significant enhancements of the wingman are achieved, in terms of the lift-to-drag ratio, pitching, rolling, and yawing moments in steady states, but the static stabilities are reduced as unbalanced moments. Moreover, compared with a single aircraft, the unsteady sinusoidal motions indicate that the dynamic aerodynamics and its corresponding dynamic derivatives change in a much more complex manner. It is concluded that the initial angle of attack and distance in the formation flight are the main factors to evaluate the effect, which should be monitored and adjusted in real time for better use of the profit of formation, especially in dynamic maneuvering.

Keywords: computational fluid dynamics (CFD); dynamic stability derivatives; formation flight; static aerodynamics; sliding mesh.

Nomenclature

C_L	=	lift coefficient
C_d	=	drag coefficient
C_{mx}	=	rolling moment coefficient
C_{my}	=	pitching moment coefficient
C_{mz}	=	yawing moment coefficient
C_{m_0}	=	initial pitching moment coefficient
$C_{m\dot{\alpha}}$	=	derivative of pitching moment coefficient with respect to $\dot{\alpha}$
$C_{m\alpha}$	=	derivative of pitching moment coefficient with respect to α
C_{mq}	=	derivative of pitching moment coefficient with respect to q

$C_{m\dot{q}}$	=	derivative of pitching moment coefficient with respect to $\dot{q}$
C_{ref}	=	mean aerodynamic chord
$\boldsymbol{E}$	=	total energy per unit mass
$\boldsymbol{F}$	=	inviscid component of the flux vectors
$\boldsymbol{F_v}$	=	viscous flux vector
k	=	reduced frequency
Ma	=	Mach number
U	=	$(u,v,w)^T$, Cartesian velocity vector
q	=	pitching angular velocity
$\dot{q}$	=	time derivative of pitching angular velocity
Re	=	Reynolds number
t	=	time
V	=	flight velocity
V_v	=	control volume
W	=	vector of conserved variables
x_i	=	longitudinal offset between the aircrafts in formation flight
y_i	=	lateral offset between the aircrafts in formation flight
z_i	=	vertical offset between the aircrafts in formation flight
α	=	angle of attack
α_0	=	angle of attack of steady state
α_m	=	amplitude of sinusoidal motion
$\Delta\alpha$	=	change in α
$\dot{\alpha}$	=	time derivative of α
θ	=	pitching angular
θ_0	=	amplitude of pitching angular
$\dot{\theta}$	=	time derivative of pitching angular
ω	=	frequency of sinusoidal motion
$\hat{\Delta}$	=	higher order term
ρ	=	density

INTRODUCTION

In recent years, the unmanned combat aerial vehicles (UCAVs) attract a great deal of attention and have widely been used in various fields with the advantages of small volume, light weight, and high maneuverability. In particular, the fly wing UCAV (Richard & Steven, 2001) has become one of the most attended flight vehicles due to its unique characteristics of higher lift-to-drag ratio and lower observability. However, there are still many disadvantages for the single UCAV. For example, the operation range can be limited to miss the target for the reconnaissance UCAV, whereas the poor hitting is always a difficult territory for the attacking one.

In order to overcome the above issues, a new idea of formation flight is developed, which has been conventionally applied in space vehicles for the purpose of reducing the launch costs of satellites and achieving multidirectional views for observation. Based on this concept, several UCAVs can be formatted following a certain pattern and remain the relative position during the flying. As a result, these UCAVs can then be used to finish more complicated tasks with all-round and three-dimensional effect. The benefits of flying in adjacent formation mainly arise from the disturbance-velocity induced by the vortices preliminary from the wingtip of the leading aircraft. If the trailing aircraft or the wingman is in the right position, the disturbance produced by the leader will increase the upwash and the local angle of attack for the wingman, which will enhance the aerodynamic efficiency of the whole formation that cannot be achieved with one single aircraft. However, the wake upwash from the leading aircraft affects not only the lift and drag characteristics, but also the unbalanced pitching, rolling, and yawing moments, which are detrimental to the static or dynamic stability and further lead to complex influences on the trailing aircraft control.

In order to evaluate the aerodynamic phenomena during formation flight, many scholars have carried out various methods both on numerical simulation and experiments. Bangash *et al.* (2006) and Wang *et al.* (2003) presented a vortex-lattice numerical scheme to investigate the effect of spatial offset between the leading and trailing wings. Their analysis data revealed that the spatial offset and angle of attack of the leading wing had significant impact on the wingman. However, the method is simple and not accurate. Barnes *et al.* (2000) analyzed the stream-wise oriented vortex interactions for two wings in close proximity by using CFD methods. The results indicate the detailed static aerodynamic characteristics of the formation, but ignore the dynamic stability analysis. Insaswa *et al.* (2003) had done similar work through wind tunnel tests, which was also limited to the static effect of the vortex from the leading wings. Atilla *et al.* (2003) and Blake (2000), respectively, developed models for simulation of close formation flight with the wind tunnel tests. These models could fit the aerodynamic forces and moments in limited cases, but a detailed research should be further proposed to improve the dynamic analysis of the wingman. Wanger *et al.* (2001) adopted different methods to simulate the drag reduction in formation fight, which discussed the mechanism of change of static aerodynamic characteristics. However, none of the research was related to dynamic stability of the trailing aircraft (Ralph &William, 1997; Esteban, 2001).

As mentioned above, formation flight with fly wings can be widely used in both military and civil areas to dramatically improve the efficiency and accuracy of different applications. However, the unbalanced moments caused by the leading aircraft will bring complex flight dynamics

problems during the formation. Unfortunately, few articles have analyzed the static and dynamic characteristics of the wingman in detail simultaneously. In this paper, a new method is proposed to change the situation with CFD. The static and dynamic flow fields are accurately calculated by using sliding mesh technique, and the dynamic stability derivatives are identified with the small oscillation method for all the directions. The effect of distance between the leading and trailing fly wings and initial angle of attack has been systematically analyzed. Finally, a conclusion is made and the future work intentions are commented on, and the research in this paper can provide technique support for the control and aerodynamic analysis of actual formation flight.

NUMERICAL METHOD

A. Governing equation

The commercial software "FLUENT 2014" is chosen to simulate the steady and unsteady cases in this paper. As we know, this software provides various physical models for solving different fluid flow problems, and it has been verified to be of high precision and robust in engineering.

The 3D Reynolds average N-S equation used to describe the flow field is expressed as

$$\frac{\partial}{\partial t}\iiint_{V_v} W dV_v + \iint_{\partial V_v} \boldsymbol{F} \cdot \boldsymbol{n} ds = \frac{1}{\mathrm{Re}} \iint_{\partial V_v} \boldsymbol{F}_v \cdot \boldsymbol{n} ds \tag{1}$$

where V_v is the control volume, $W = (\rho, \rho u, \rho v, \rho w, \rho E)^T$ is the vector of conserved variables, ρ is the density, and u, v and w are the components of velocity given by the Cartesian velocity vector $U = (u, v, w)^T$. The total energy per unit mass is E. F denotes the inviscid component of the flux vectors, while Fv is the viscous flux vector, which contains terms of the heat flux and viscous forces exerted on the body. Re is the Reynolds number.

The two-equation turbulence model, called shear-stress transport (SST) $k-\omega$ model, is used in all the cases of this paper. Developed by Menter (1994), the model effectively blends the robust and accurate formulation of the $k-\omega$ model in the new-wall region with the free-stream independence of the $k-\varepsilon$ model in the far field. Furthermore, the modification makes the SST $k-\omega$ model more accurate and reliable for a wider class of flows than the standard $k-\varepsilon$ model.

B. Method for calculating the dynamic derivatives

Dynamic stability is one of the most important characteristics of flight dynamics, which can be represented with dynamic stability derivatives (Erkin, 2000; Robert, 2004). This concept was first introduced by Bryan (1911) and now is widely used in modeling the unsteady aerodynamic forces and design of flight control system.

The conventional method with CFD is employed to identify the dynamic derivatives in single and formation cases. Based on the small disturbance theory, the method forces the aircraft to move sinusoidally around the center of gravity, and then the unsteady aerodynamic forces and moments can be described as linear functions of several parameters (Soo et al., 2002; Green et al., 2004). This method is introduced through the calculation of longitudinal dynamic derivatives, and the unsteady pitching moment coefficient related to the angle of attack α, pitching angular velocity q, and the rate of these two variables $\dot{\alpha}$ and $\dot{q}$ is expressed as

$$C_m = C_{m0} + C_{m\alpha}\Delta\alpha + C_{m\dot{\alpha}}\Delta\dot{\alpha} + C_{mq}q + C_{m\dot{q}}\dot{q} + \hat{\Delta}(\Delta\alpha, q) \tag{2}$$

When discarding the high order terms $C_{m\dot{q}}\dot{q}$ and $\hat{\Delta}(\Delta\alpha, q)$, Eq. (2) is simplified to

$$C_m = C_{m0} + C_{m\alpha}\Delta\alpha + C_{m\dot{\alpha}}\Delta\dot{\alpha} + C_{mq}q \tag{3}$$

Combined with harmonic motion defined as

$$\begin{cases} \theta = \theta_0 \sin(\omega t) \\ \dot{\theta} = \omega\theta_0 \cos(\omega t) = q \\ \ddot{\theta} = -\omega^2\theta_0 \sin(\omega t) = \dot{q} \\ \Delta\alpha = \theta = \theta_0 \sin(\omega t) \\ \Delta\dot{\alpha} = \dot{\theta} = \omega\theta_0 \cos(\omega t) \end{cases} \tag{4}$$

Eq. (3) can then be rewritten as

$$C_m = C_{m0} + (C_{m\alpha} - \omega^2 C_{m\dot{q}})\theta_0 \sin\omega t + (C_{m\dot{\alpha}} + C_{mq})\omega\theta_0 \cos\omega t \tag{5}$$

When $\omega t = 2n\pi$ and $\omega t = 2n\pi + \pi/2$, Eq. (5) can be expressed as

$$C_{m\dot{\alpha}} + C_{mq} = \frac{C_{m\omega t=2n\pi} - C_{m0}}{k\theta_0} \tag{6}$$

$$C_{m\alpha} - \omega^2 C_{m\dot{q}} = \frac{C_{m\omega t=2n\pi+\pi/2} - C_{m0}}{\theta_0} \tag{7}$$

where $k = \omega c / 2V_\infty$ is the non-dimensional reduced frequency of the applied motion, and $C_{m\dot{\alpha}} + C_{mq}$ is the combined dynamic derivative since $\dot{\alpha}$ and q are difficult to separate when the freestream velocity is unchanged. Moreover, $C_{m\alpha} - \omega^2 C_{m\dot{q}}$, called in-phase derivative, is comprised of a static derivative $C_{m\alpha}$ and a rotational derivative $C_{m\dot{q}}$.

Sliding mesh is adopted to simulate the dynamic motion in all unsteady cases, which is a special case of general dynamic mesh motion, wherein all the cells move rigidly in a specified dynamic zone. In this technique, two or more cell zones are used, and each cell zone is bounded by at least one interface zone where it meets the opposing cell zone. The interface zones of the adjacent cell zones are associated with one another to form a mesh interface. During the unsteady calculation, the cell zones slide relative to one another along the interface in discrete steps. Because the mesh motion in this dynamic mesh formulation is rigid, all cells retain their original shape and volume; see Figure 1. As a result, it is proved to be a time-consuming method to solve the multi-body motion.

It should be noted that the airfoil in Figure 1 is merely used to describe the dynamic mesh method in the paper; for that reason, the 2-dimensional airfoil can more clearly show the sliding mesh technique than the 3-dimensional configuration. The practical model is a flying wing configuration shown in the following part.

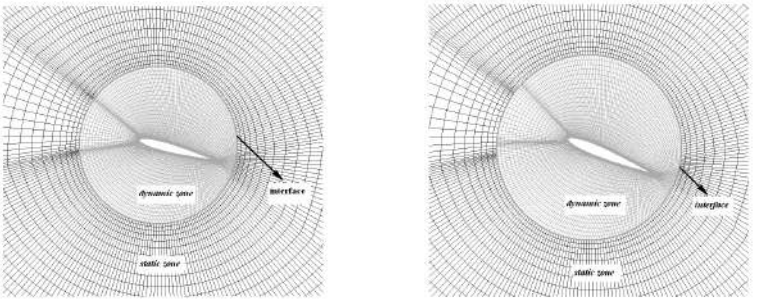

(a) Initial mesh (b) Mesh after movement

Fig. 1. Sliding mesh.

C. Validation of CFD method to calculate dynamic derivative

A generic UCAV, called SACCON "Stability and Control CONfiguration" used by an Applied Vehicle Technology Task Group (AVT-161) established by the NATO Research and Technology Organization (RTO), is adopted to verify the method. The corresponding static and dynamic aerodynamics had been carried out in the Low Speed Wind Tunnel Braunschweig (DNW-NWB) as shown in Figure 2.

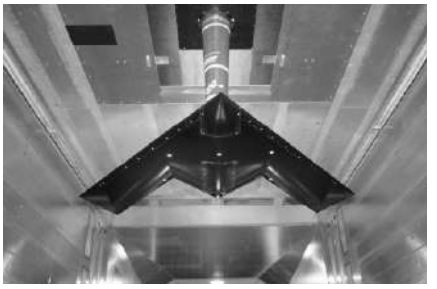

Fig. 2. SACCON model in the closet test section of the Low Speed Wind Tunnel (DNW-NWB) (Dan et al., 2010).

The model contains a lambda wing with a leading edge sweep angle of 53^{o}, shown in Figure 3. The root chord is approximately 1m and the wing span is 1.53m, while the mean aerodynamic chord is 0.479m and the reference wing area is $0.77m^2$. The moment reference point (MRP) is located at 0.6m from the head of the wing, and the point of rotation (POR) for dynamic testing is 0.255414m behind the MRP. More detailed description can be seen in Dan *et al.* (2010).

The commercial software ICEM CFD is used to generate the computational mesh with a total size of 4 million cells in the dynamic zone and 1.5 million cells in the out zone (shown in Figures 4–6). The extent of the boundary layer is 4.9mm and the thickness of the first layer is 0.0036mm, which indicate that the largest value of y^+ does not exceed the value of 1.15. The mesh cells are clustered around the leading edges, and the volume mesh has enhanced density around the aircraft in order to insure adequate resolution of flow filed.

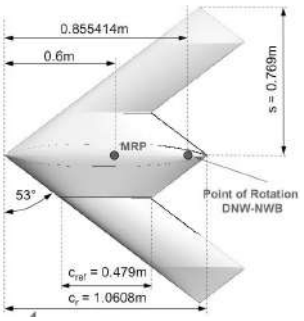

Fig. 3. Geometric parameters of the SACCON UCAV configuration (Dan *et al.* 2010).

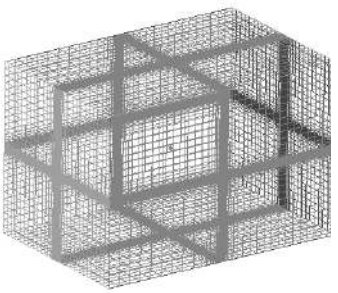

Fig. 4. Computational mesh of a static domain.

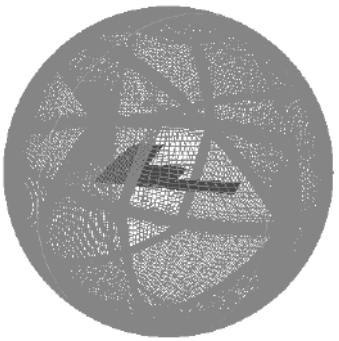

Fig. 5. Computational mesh of a dynamic domain.

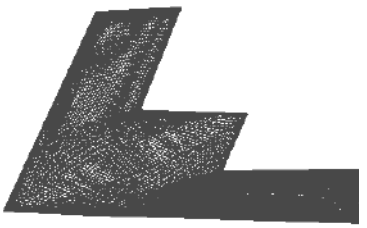

Fig. 6. Computational mesh of surface.

The validation case for a single plane without a sting is taken with the same conditions as the wind tunnel tests; see Table 1. Based on the sliding mesh technique, the unsteady pitching moment coefficient and its hysteresis loops are, respectively, shown in Figures 78-. The longitudinal combined dynamic derivative is calculated in Table 2. Compared to the wind tunnel testing data (Cummings et al., 2010), an error of 5.83% indicates good accuracy of the method.

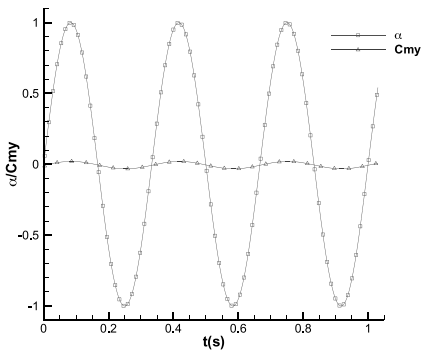

Fig. 7. Unsteady pitching moment coefficient

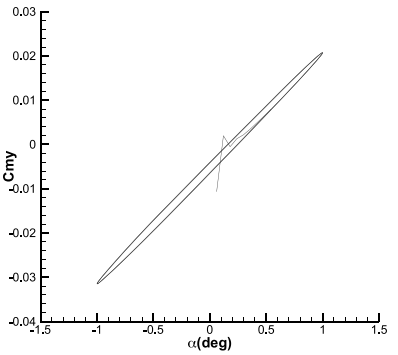

Fig. 8. Hysteresis loops of pitching moment coefficient

Table 1. Simulation conditions.

Parameters	Values
Mach number	$Ma = 0.147$
Reynolds number based on mean aerodynamic chord	$\mathrm{Re}_c = 1.64 \times 10^6$
Initial angle of attack	$\alpha_0 = 0$ degree
Reduced frequency	$k = \omega C_{ref} / 2V = 0.0903$
Sinusoidal motion	$\Delta\alpha = 1^o \sin(\omega t) = 1^o \sin(6\pi t)$

Table 2. Longitudinal combined dynamic derivative.

Initial angle of attack	$C_{m\dot{\alpha}} + C_{mq} - cal$	$C_{m\dot{\alpha}} + C_{mq}$ – exp (Cummings et *al*. 2010)	error
0	-1.20	-1.13	5.83%

MODEL OF FORMATION CALCULATION

Two-flight-vehicle formation is studied in this work to analyze the static and dynamic aerodynamic characteristics of wingman caused by a leading aircraft. The two UCAVs are identical to each other with the same configuration and initial flying attitude. A schematic diagram is shown in Figure 9, where (x_i, y_i) represents the longitudinal and lateral offsets between the two aircrafts. Various groups of values, (4, 1.5), (4, 2), (3, 1.5), and (3, 2), are used to investigate the effect of different displacements, which are illustrated in Figure 10.

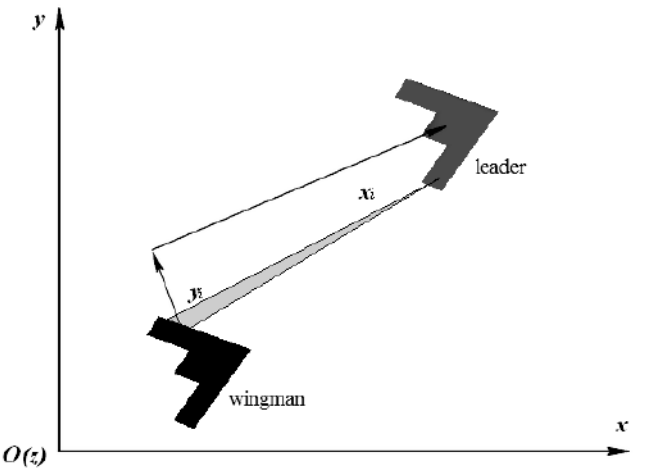

Fig. 9. Formation with two SACCON UCAVs.

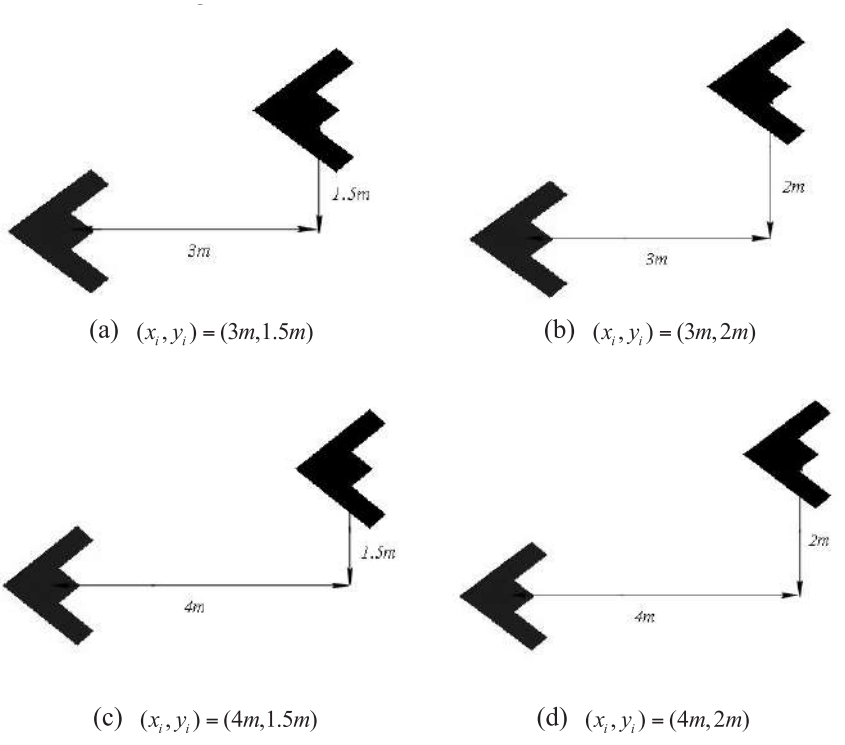

(a) $(x_i, y_i) = (3m, 1.5m)$ (b) $(x_i, y_i) = (3m, 2m)$

(c) $(x_i, y_i) = (4m, 1.5m)$ (d) $(x_i, y_i) = (4m, 2m)$

Fig. 10. Various groups of offsets between two aircrafts.

STATIC AERODYNAMIC CHARACTERISTICS

The conditions of computing the static aerodynamics of the wingman are the same as those of the single aircraft calculation. Figure 11 presents the comparison of static aerodynamic forces and moments between the wingman and single aircraft. The results demonstrate that the leader produces significant interference to the aerodynamics of wingman.

Compared to a single aircraft, the lift coefficient of wingman increases, while the drag coefficient decreases at the same angle of attack, which indicates that the formation can enhance the aerodynamic performance of the wingman with maximum improvement in the lift-to-drag ratio of about 23%. Meanwhile, the distance of y_i –dimension has greater effect on the aerodynamic of wingman than that of the $\boldsymbol{x_i}$-dimension. When (x_i, y_i) equals to $(3m, 1.5m)$, the lift-to-drag ratio of wingman at 8 degrees angle of attack increases by 23%, while only 8.5% made if y_i extends to $2m$. To make full use of formation flight profit, the interference range and formation distance should be monitored and adjusted in real time.

The pitching moment coefficient and its slope of the wingman are larger than those of single fly wing aircraft. This will reduce stability characteristics for the reason that it is always a certain statically unstable system for this configuration. The lateral and directional moment

change to positive values at the range of angle of attack in Figure 11(c) and Figure 11(d) under influence of upwash from the leading wing and vortex interactions. The result indicates a significant increase of rolling and yawing moments for α within almost the entire range of flight cases.

Figure 12 displays pressure coefficients of several wing sections under normal and formative circumstances. The results show that the wing-tip vortex of the leading aircraft has been strongly enhanced with the increase of local angle of attack, and the lift also partially increases at the front of wing section. However, this effect is not remarkable at $\alpha = 0$ due to the fact that the flow field is relatively stable at small angles of attack, and then the wake is not very strong and will be quickly dissipated during the downward motion. This is the reason why minute differences happen in pressure distribution at sections $y = -0.72$, $y = -0.7$, and $y = -0.6$. Apparently, the aerodynamic configuration and size also significantly affect the wing-tip vortex intensity of leader. For the SACCON fly wing model used in this work, the inscribed modification on the wingtip has alleviated the effects of downwash.

When the angle of attack is increased to 5 and 10 degrees, the tip vortices of the leader become strong, and their influence ranges transform from the front to the back part of the wing section of wingman. Consequently, the lift of left part of the trailing aircraft close to the leader increases, and its pitching moment is also produced around the moment center. Moreover, due to the asymmetric lift characteristics, a positive rolling moment is also leaded. Furthermore, the reduced drag of the left wing for wingman causes positive yaw moment around the center of gravity.

It is obvious that the static aerodynamics of SACCON in formation flight is mainly affected by the distance of y_i–dimension, which can be detailed in Figure 12. The pressure coefficients are apparently different from each other when $(x_i, y_i) = (4m, 1.5m)$ and $(x_i, y_i) = (4m, 2m)$. Actually, the position of vortex is not at the tip of the aircraft but is in favor of the fuselage due to the additional upwash velocity. The distance of y_i represents whether the wingman locates in the range of upwashing wake of the leading aircraft. In comparison to the effect of distance of y_i, the wing-tip vortex converged by small ones from the up-surface and tip of the wing attenuates slightly, where the wingman can be influenced within a long range of x_i distance.

Paying special attention to the cases at $y_i = 1.5m, \alpha = 12^o$, the yawing moment coefficients of the wingman suddenly drop from positive to negative values. This is mainly because that flow separation appears on the surface of the fly wing configuration at this angle of attack, then the wing tip vortex of the leading aircraft is affected, to be very different with small angle of attack, and the shear effect of y_i direction is much stronger than that of x_i direction. At the same time, we can see that the yawing moment coefficients are also affected at $y_i = 2m, \alpha = 12^o$, and the growth rate is slowed down.

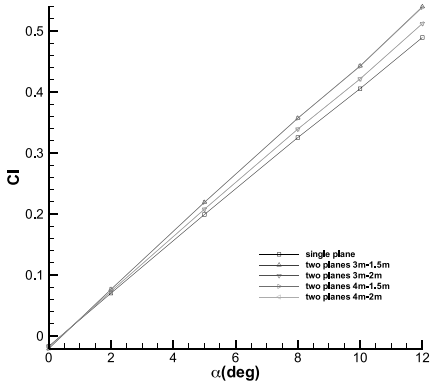

(a) Lift coefficients

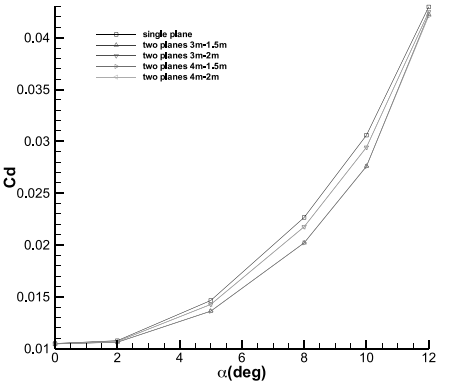

(b) Drag coefficients

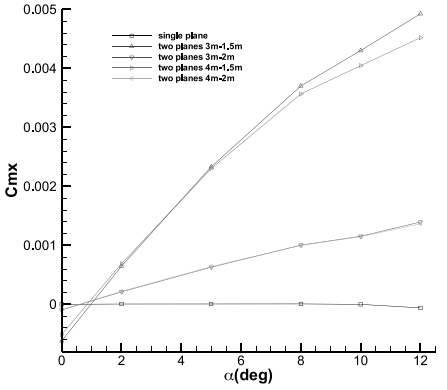

(c) Rolling moment coefficients

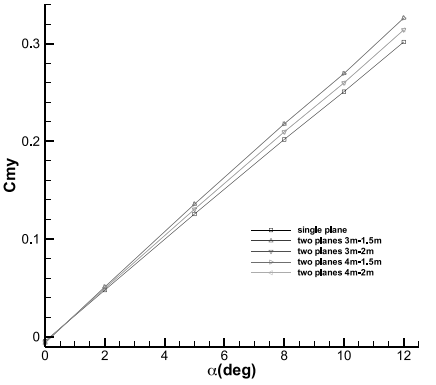

(d) Pitching moment coefficients

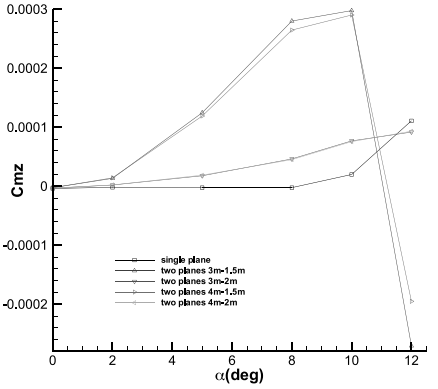

(e) Yawing moment coefficients

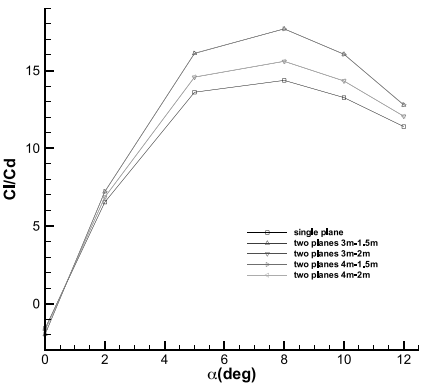

(f) Lift-to drag ratios

Fig. 11. Static aerodynamic forces and moments coefficients.

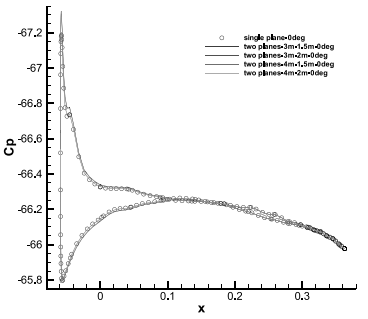

(a) Pressure Coefficient at y=-0.6m ($\alpha_0 = 0$)

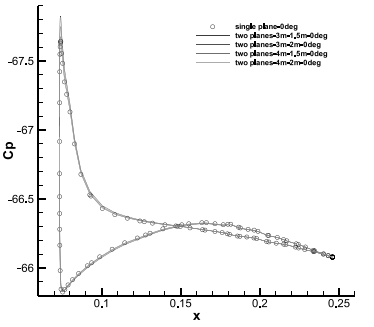

(b) Pressure Coefficient at y=-0.7m ($\alpha_0 = 0$)

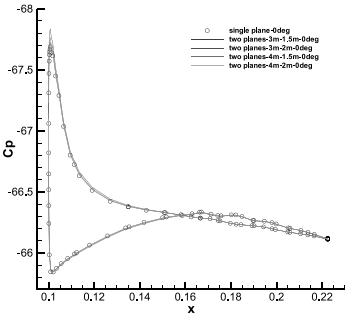

(c) Pressure Coefficient at y=-0.72m ($\alpha_0 = 0$)

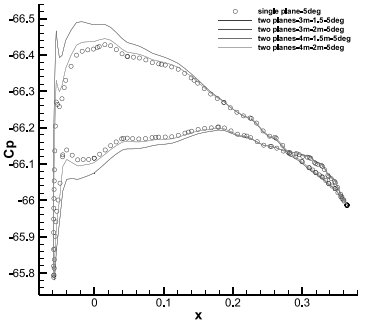

(d) Pressure Coefficient at y=-0.6m ($\alpha_0 = 5$)

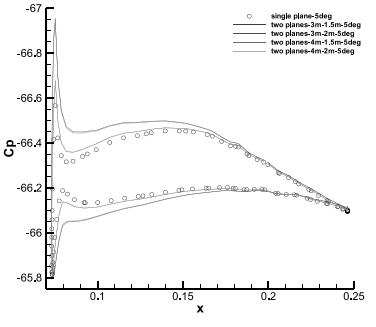

(e) Pressure Coefficient at y=-0.7m ($\alpha_0 = 5$)

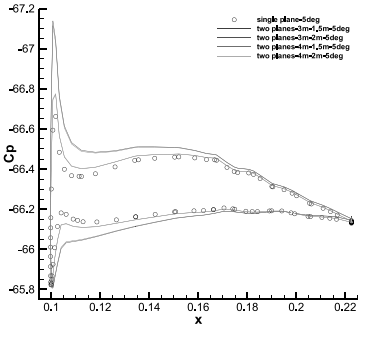

(f) Pressure Coefficient at y=-0.72m ($\alpha_0 = 5$)

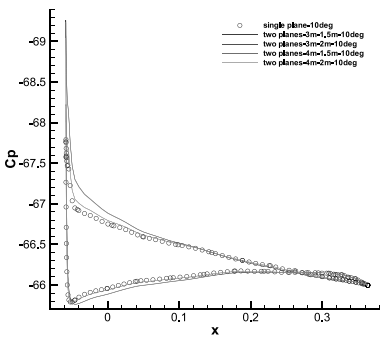

(g) Pressure Coefficient at y=-0.6m ($\alpha_0 = 10$)

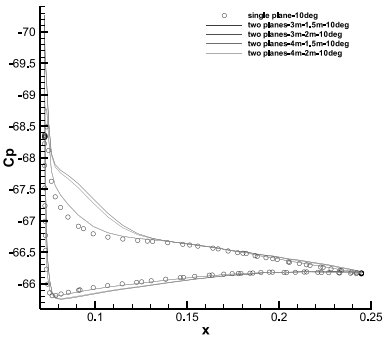

(h) Pressure Coefficient at y=-0.7m ($\alpha_0 = 10$)

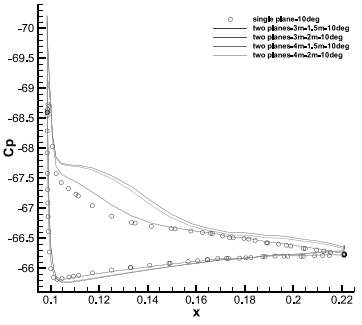

(i) Pressure Coefficient at y=-0.72m ($\alpha_0 = 10$)

Fig. 12. Pressure coefficients at different sections.

DYNAMIC AERODYNAMIC CHARACTERISTICS

5.1 Longitudinal dynamic aerodynamics

Based on the unsteady aerodynamic analysis method using sliding mesh, the longitudinal dynamic characteristics of wingman with different formation patterns can be calculated. The Mach number is Ma = 0.1479, and the Reynolds number based on mean aerodynamic chord C_{ref}= 0.479 m is defined as Re = 1.64 × 10^6. To identify the combined dynamic derivatives, the wingman should be imposed to move sinusoidally around its center of gravity. The motion is described as $\alpha = \alpha_0 + \alpha_m \sin(\omega t) = \alpha_0 + 1^o \sin(6\pi t)$, where α_0 denotes the initial angle of attack, and the reduced frequency is $k = \omega C_{ref} / 2V = 0.0903$.

The unsteady resulting variation in pitching moment coefficients experienced by the wingman SACCON UCAV is presented in Figures 13a–c, which shows a marked difference between the normal and formation flight as α_0 increases. All the hysteresis loops of unsteady moments are counterclockwise, which indicates that the wingman in both normal and formation systems exhibits dynamic damping characteristics.

The longitudinal combined dynamic derivatives are given in Figure 14. Due to the effect of the leader aircraft, the trend of wingman's dynamic stability derivative is clearly changed. For the normal single aircraft, the absolute values of longitudinal combined dynamic derivative firstly increase and then decrease, as well as the dynamic damping. However, these values of the trailing aircraft in formation flight always decrease as the increment of the initial angle of attack, which indicates diminished longitudinal dynamic damping with the growing wake of the leading aircraft.

When $\alpha_0 = 0$, the wingtip vortex of leader is weak, and the absolute values of dynamic derivative of trailing aircraft in formation flight are bigger than those of the normal single aircraft. We clearly find that the impacts from leader wake increase the dynamic damping of wingman, and the distance of x_i is the main factor between the two planes. As α_0 increases to 5 degrees, the strength of vortex enhances and all the longitudinal dynamic damping of wingman decreases. Furthermore, the corresponding absolute values of derivatives and the distance of x_i and y_i can change the longitudinal dynamic stability. Under the condition of angle of attack, the vortex caused by leader aircraft is much stronger. As a result, the trailing aircraft can be deeply interfered in a larger range, especially along the y_i direction. The effect is that the absolute values of longitudinal dynamic derivatives of wingman are bigger and the dynamic damping is smaller in the y_i direction, while the adverse effect leads to smaller dynamic damping.

Taken together, combined with the effect of wingtip vortex of leader aircraft, the unsteady flow field of the wingman in sinusoidal motion is much more complicated than that of the normal flight, and the distance of x_i and y_i has different influences on the dynamic stability of the trailing aircraft. Thus, to achieve the best profit of actual formation flight, the change in distance and angle of attack should be evaluated in detail, and the pattern of formation also should be more elaborately adjusted in real time.

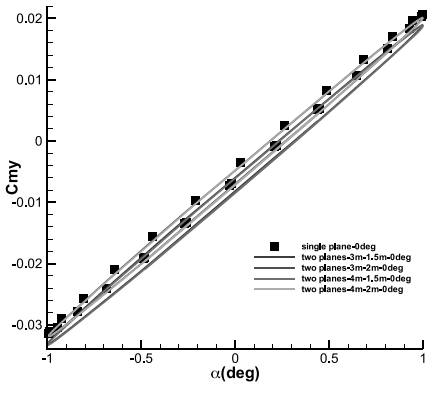

Fig.13a. Hysteresis loops at $\alpha_0 = 0$.

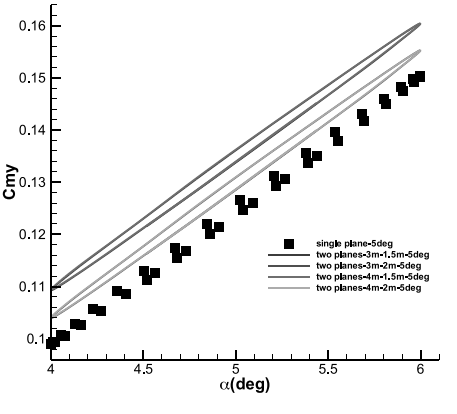

Fig. 13b. Hysteresis loops at $\alpha_0 = 5^o$.

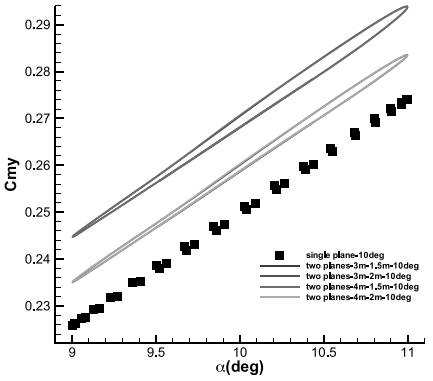

Fig. 13c. Hysteresis loops at $\alpha_0 = 10^o$.

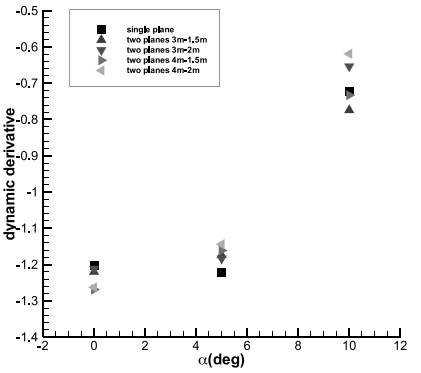

Fig. 14. Longitudinal combined dynamic derivatives.

The same free stream conditions are used to simulate the lateral cases in normal and formation flight. The unsteady aerodynamics are calculated with the sinusoidal motion expressed as $\varphi = \varphi_m \sin(\omega t) = 1^o \sin(6\pi t)$, and the reduced frequency is $k = \omega B_{ref} / 2V = 0.2884$, where B_{ref} is wingspan.

Figures 15a–c demonstrate the unsteady rolling moment coefficients of the wingman at three initial angles of attack: 0, 5, and 10°, respectively. At the incidence of 0, all the counterclockwise hysteresis loops indicate dynamic damping characteristics of the system, while the distance of y_i produces more influence on the unsteady aerodynamics than that of x_i. At 5° angle of attack, a strong vortex from the wingtip of the leader makes more differences when comparing the unsteady loops to those of the single aircraft. Here we find that the distance of y_i still holds a leading position for affecting the aerodynamics of the trailing aircraft. By the time the incidence reaches 10°, a much stronger wake extends axially over the wingman, and the unsteady rolling moments are significantly changing with the different displacements of y_i.

The predicted rolling combined dynamic derivatives denoted as $C_{l\beta} \sin\alpha + C_{lp}$ of all the cases are shown in Figure 16. Similar to the normal single aircraft, the absolute values of the derivatives of the wingman in formation flight get smaller as the incidence is increased. Compared to the single aircraft, at angles of attack 0 and 10°, the absolute derivative values in formation become smaller, while an adverse change happens when the angle of attack is 5°, which indicates increments of dynamic damping in these cases.

Due to the fact that the lateral-directional is coupled, we need to focus on the unsteady yawing moment and the cross combined dynamic derivatives $C_{n\beta} \sin\alpha + C_{np}$ introduced by the rolling motion; see Figures 17a–c and Figure 18. The results show that the wake of the leader is not so strong at a 0 angle of attack. Furthermore, there is no significant difference in both the aerodynamic moments and derivatives between the aircraft with and without formation. However, the cross dynamic damping at angle of incidence 5° grows as the distance of y_i is increased, which is illustrated with larger absolute values of the dynamic derivative of the wingman. Moreover, the variations of cross dynamic damping can be more complicated when the angle of attack reaches up to 10° with the phenomena that smaller y_i value produces divergence characteristics, while the larger one makes the damping moment.

Overall, both the rolling and yawing moments of the wingman in lateral unsteady motion with formation are different from those of the single aircraft, and the longitudinal cases are similar. The distance of y_i is one of the main factors in formation flight at different initial angles of attack.

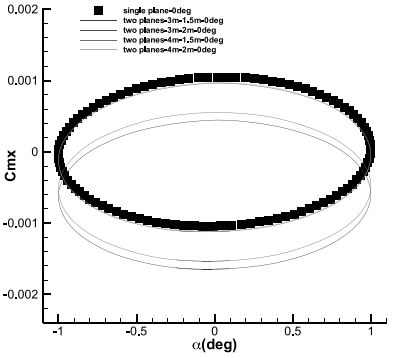

Fig. 15a. Rolling moment coefficients at $\alpha_0 = 0$.

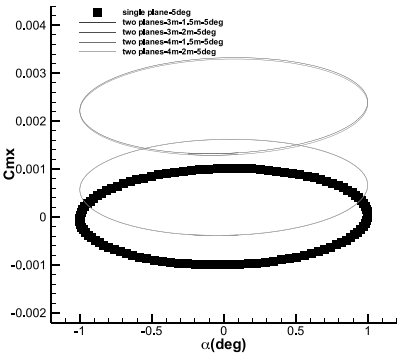

Fig. 15b. Rolling moment coefficients at $\alpha_0 = 5^o$.

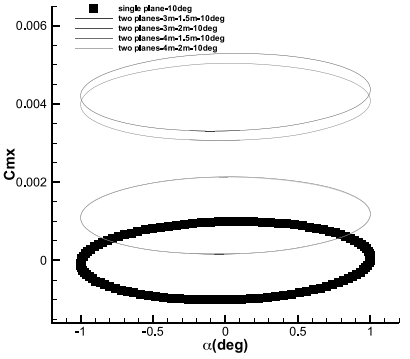

Fig. 15c. Rolling moment coefficients at $\alpha_0 = 10^o$.

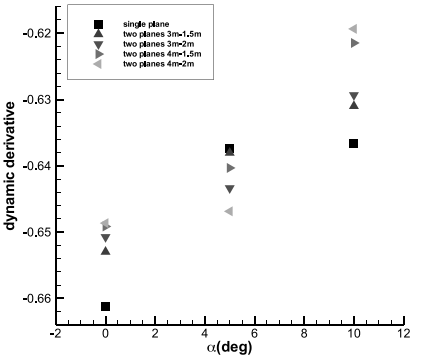

Fig. 16. Combined dynamic derivatives of rolling moment coefficients.

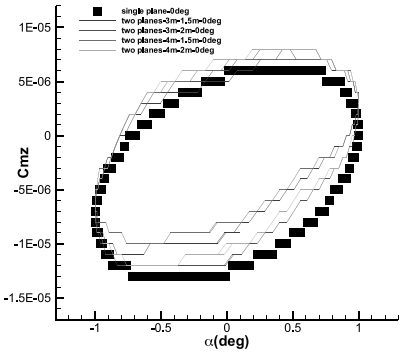

Fig. 17a. Yawing moment coefficients at $\alpha_0 = 0$.

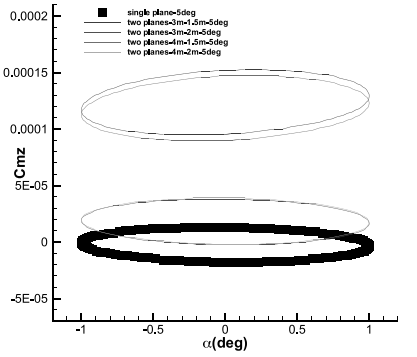

Fig. 17b. Yawing moment coefficients at $\alpha_0 = 5^o$.

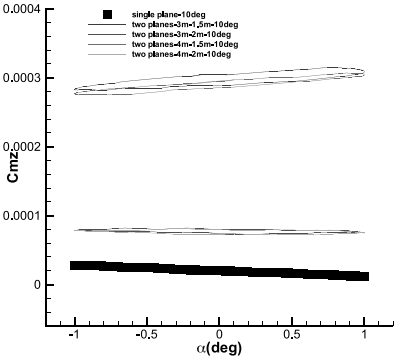

Fig. 17c. Yawing moment coefficients at $\alpha_0 = 10^o$.

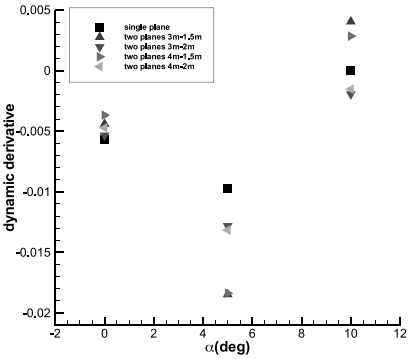

Fig. 18. Cross combined dynamic derivatives of yawing moment coefficients.

5.3 Directional dynamic aerodynamics

The unsteady sinusoidal motion to simulate the directional dynamic aerodynamics is expressed as $\psi = \psi_m \sin(\omega t) = 1^o \sin(6\pi t)$, with the reduced frequency $k = \omega B_{ref} / 2V = 0.2884$ at three initial angles of attack: 0, 5, and 10°.

Figures 19a–c display the unsteady rolling moment coefficients of trailing aircraft in normal and formation flights. The cross rolling combined dynamic derivatives are shown in Figure 20. It is clear that the unsteady aerodynamic moments are different from each other in these cases, though the derivative values of the wingman correspond closely to those of the single aircraft at angle of attack 0. When $\alpha_0 = 5^o$, all the dynamic derivatives are positive values, which indicates that the dynamic systems exhibit divergence characteristics. The distances of y_i also make great effect on the aerodynamics of the wingman as the hysteresis loops in the formation flight deviate from the normal case. The dynamic characteristics at 10° angle of attack are almost the same as those of $\alpha_0 = 5^o$, but the negative and positive values of the cross combined dynamic derivatives state that the unsteady motion may be either damping or divergence system with different distances of y_i.

The unsteady yawing moment coefficients and the corresponding combined dynamic derivatives are, respectively, shown in Figures 21a–c and Figure 22. Unlike the cases done by other institutions, the initial angle of attack equals 0, and the derivative values are mainly affected by the values of x_i. When the angle of attack reaches up to 5 and 10°, the dynamic aerodynamics are closely related to y_i. Negative damping caused by the wake of the leader with larger y_i values leads to positive values of stability derivatives at $\alpha_0 = 10^o$, while the opposite effect is produced with smaller y_i values.

As mentioned above, the distance of formation has significant influence on the directional aerodynamics of the wingman, which becomes stronger as the initial angle of attack is increased. In general, the distance of y_i plays a more important role in the influence factors of formation flight during yawing motion. Because of poor directional stability for the flying wing UCAV, we should take more care of dynamic analysis in formation flight.

Concluding the static and all the dynamic results, we suggest that the longitudinal offsets bring more obvious influences on dynamic performances than those of static cases. The main reason is that the change of wingtip vortex of the leading aircraft in static cases is not significant along the x_i direction, while the wingman can be affected by the shear effect of the wingtip vortex along the z_i direction in dynamic motions. Moreover, the flow flied from the wingman can also affect the leading aircraft in subsonic flight. Therefore, the differences between static and dynamic cases are the result of a combination of several factors.

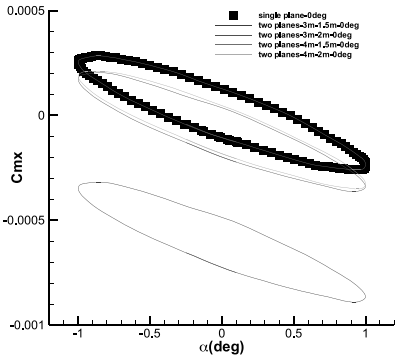

Fig.19a. Rolling moment coefficients at $\alpha_0 = 0$.

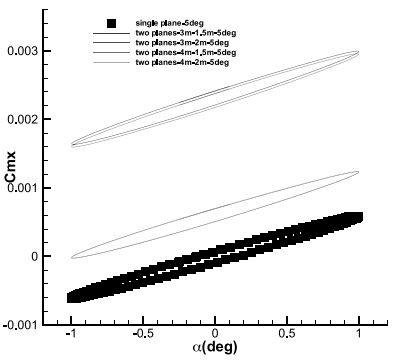

Fig. 19b. Rolling moment coefficients at $\alpha_0 = 5^o$.

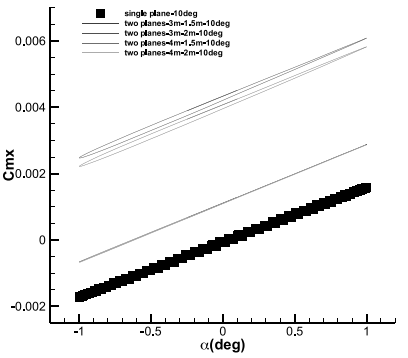

Fig. 19c. Rolling moment coefficients at

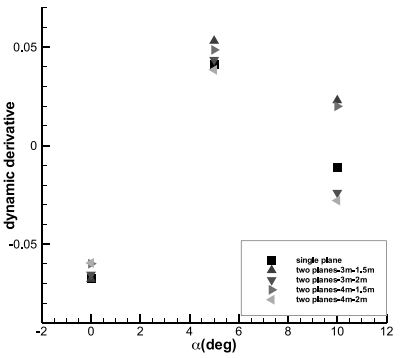

Fig. 20. Cross rolling dynamic derivatives.

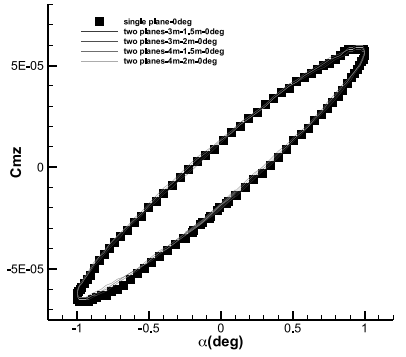

Fig. 21a. Yawing moment coefficients at $\alpha_0 = 0$.

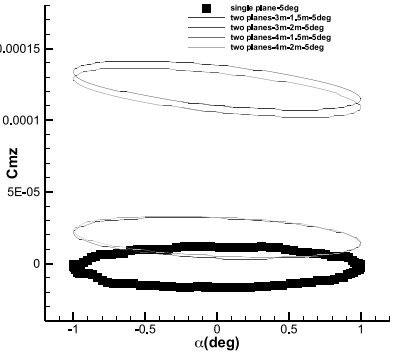

Fig. 21b. Yawing moment coefficients at $\alpha_0 = 5^o$.

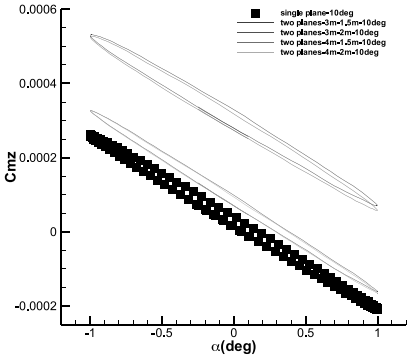

Fig. 21c. Yawing moment coefficients at $\alpha_0 = 10^o$.

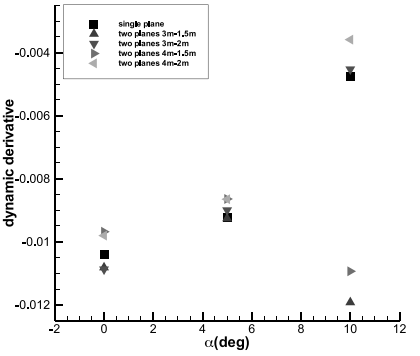

Fig. 22. Yawing dynamic derivatives.

CONCLUSIONS

A computational fluid dynamics (CFD) method based on a sliding mesh is proposed herein to calculate the static and dynamic aerodynamics of the trailing aircraft in both formation and normal single flights. Moreover, the dynamic stability derivatives of all directions are identified with a conventional method. The static and dynamic aerodynamic characteristics of the trailing aircraft are obviously changed and are different from those of the single one in a normal flight. The reason behind this is the coexistence of wingtip vortex caused by the leader.

For static cases, the steady-state result shows that significant enhancements are made on both the lift-to-drag ratio and the moments of pitching, rolling, and yawing, which leads to desirable lift and drag effects, while a reduction in static stability of the fly wing wingman is exhibited with the unbalanced moments. Furthermore, the wingman's dynamic aerodynamics in longitudinal and lateral direction are affected significantly with the effect of the wake, as well as the combined dynamic stability derivatives that indicate the dynamic damping of the system. No matter longitudinal or lateral directional static and dynamic motions of the trailing aircraft in formation flight, the initial angle of attack and distance are the main factors to evaluate the effects. The initial angle of attack can represent the strength of the vortex, while the distance of mainly describes affected areas for the wingman.

In conclusion, to take good advantage of the effect of leading aircraft, the distance and angle of attack of the wingman should be monitored and adjusted in real time. Furthermore, the detailed method and analysis for the formation of flying wing UCAVs can provide efficient tools for the advanced flight control and design. Further work will involve more accurate LES/DES simulations to capture the vortex of the leading aircraft in detail, especially for the formation flight beyond small angle of attack. The single dynamic derivative and unsteady aerodynamic model of the wingman should also be considered. Finally, the flight testing with scaled model will be studied to validate all the numerical methods.

ACKNOWLEDGMENTS

The authors would like to acknowledge the support of Grant No. 2015ZA53013 from the Aeronautical Science Foundation of China.

REFERENCES

Richard, M. W. & Steven, X. S. 2001. Flying wings/ Flying fuselages, 39th Aerospace Sciences Meeting and Exhibit, Reno, Nevada, USA, pp: 1 - 27.

Bangash, Z. A., Sanchez, R. P. & Ahmed, A. 2006. Aerodynamics of formation flight, Journal of Aircraft. 43(4), pp: 907 - 912.

Wang, Z. C. & Mook, D. T. 2003. Numerical aerodynamic analysis of formation flight, 41st AIAA Aerospace Sciences Meeting and Exhibit, Reno, Nevada, USA, pp:1 - 12.

Barnes, C. J., Visbal, M. R. & Gordnier, R. E. 2000. Analysis of stream-wise-oriented vortex interactions for two wings in close proximity, Physics of Fluid. 23(1), pp. 1 - 23.

Insaswa, A., Mori, F. & Asai, M. 2003. Detailed observations of interactions of wingtip vortices in close-formation flight, Journal of Aircraft. 49(1), pp: 206 - 213.

Atilla, D. & Sriram, V. 2005. Modeling of aerodynamic coupling between aircraft in close proximity, Journal of Aircraft. 42(7), pp: 941 - 945.

Blake, W. 2000. An aerodynamic model for simulation of close formation flight, AIAA Modeling and Simulation Technologies Conference and Exhibition, Denver, CO, USA, pp: 1 - 10.

Wanger, C. G., Jacques, L. D., Blake, B. & Pachter, M. 2001. An analytical study of drag reduction in tight formation flight, AIAA Atmospheric Flight Mechanics Conference and Exhibit, Montreal, Canada, pp:1 - 11.

Ralph, P. & William, G. L. 1997. Dynamic and control of tailless aircraft, 22nd Atmospheric Flight Mechanics Conference, New Orleans, LA, USA, pp:1 - 10.

Esteban, S. 2001. Static and dynamic analysis of an unconventional plane: flying wing, AIAA Atmospheric Flight Mechanics Conference and Exhibit, Montreal, Canada, pp: 1 - 16.

ANSYS FLUENT, 2014. ANSYS Inc. http:// www.ansys.com / Products / Fluids/ ANSYS-Fluent

Menter, F. R. 1994. Two-equation eddy-viscosity transport turbulence model for engineering applications. AIAA Journal, 32(8), pp:1598 - 1605.

Erkin B. 2000. Dynamics of Atmospheric Flight, Dover, Mineola, New York. USA.

Robert F. S. 2004. Flight dynamics, Princeton University Press, USA.

Bryan G. H. 1911. Stability in aviation, MacMillan, London, UK.

Soo, H. P., Yoonsik, K. & Jang, H. K. 2002. Prediction of dynamic damping coefficients using unsteady dual-Time stepping method, 40th AIAA Aerospace Sciences Meeting & Exhibit, Reno, Nevada, USA, pp: 1- 9.

Green, L. L., Spence, A. M. & Murphy, P. C. 2004. Computational methods for dynamic stability and control derivatives, AIAA Atmospheric Flight Mechanics Conference, Reno, Nevada, USA, pp: 1 - 21.

Dan, D. V., Thomas, D. L. & Andreas, S. 2010. SACCON forced oscillation tests at DNW-NWB and NASA Langley 14×22-foot tunnel, 28th AIAA Applied Aerodynamics Conference, Chicago, Illinois, USA, pp: 1 - 25.

Cummings, R., Jirasek, A., Petterson, K. & Schmidt, S. 2010. SACCON static and dynamic motion flow physics simulation using cobalt. 28th AIAA Applied Aerodynamics Conference, Chicago, Illinois, USA, pp: 1 - 19.

Submitted: 06/06/2016
Revised : 24/04/2017
Accepted : 31/07/2017

محاكاة عددية للديناميكا الهوائية الساكنة والمتحركة في تشكيلة طيران باستخدام طائرات القتال بدون طيار (UCAVs)

بايجانج مي*، هاو زان وبايبنج شين**

* كلية الملاحة الجوية، جامعة نورث ويسترن للفنون التطبيقية، شيآن، الصين

** معهد شيان لبحوث تكنولوجيا التحكم الحديث، شيآن، الصين

الخـلاصة

تستطيع الطائرات الجوية القتالية بدون طيار (UCAVs) إنجاز العديد من المهام بكفاءة كبيرة جداً وذلك بواسطة استخدام تأثير دوامات طرف الجناح في طائرة رائدة. فبالاقتران مع تقنية التعشيق المنزلق، يناقش هذا البحث طريقة ديناميكية السوائل الحاسوبية (CFD) لمحاكاة وتحليل الخصائص الهوائية الديناميكية الساكنة والمتحركة لنماذج طائرات جوية ذات جناحين تسمى SACCON. بالإضافة إلى ذلك، تم اختبار والتعرف على المشتقات الديناميكية التي تشير إلى الاستقرار الديناميكي للطائرات في التشكيل، وتم كذلك تحليل الطائرات الفردية العادية كدراسة مقارنة. وأظهرت النتائج أنه نتيجة للأعقاب الهوائية في المقدمة، تحققت تحسينات كبيرة في طيار الجناح، من حيث نسبة الرفع إلى الكبح، وعزوم الترجيح والعطوف والانعراج في الحالات الثابتة، ولكن انخفضت الاستقرارية الثابتة كعزوم غير متوازنة. علاوة على ذلك، بالمقارنة مع طائرة واحدة، تشير الحركات الجيبية غير الثابتة إلى أن الديناميكية الهوائية المتحركة ومشتقاتها تتغير بطريقة أكثر تعقيداً. ونستخلص من ذلك أن الزاوية الأولية للهجوم والمسافة في تشكيل الطيران هي العوامل الرئيسية لتقييم التأثير الذي يجب مراقبته وضبطه في الوقت الحقيقي من أجل الاستخدام الأفضل للاستفادة من التكوين، خاصة أثناء المناورات الديناميكية.